A new interatomic potential for the ferroelectric and paraelectric phases of $LiNbO_3$

2005 J. Phys.: Condens. Matter 17 837

(http://iopscience.iop.org/0953-8984/17/6/005)

INSTITUTE OF PHYSICS PUBLISHING JOURNAL OF PHYSICS: CONDENSED MATTER

J. Phys.: Condens. Matter **17** (2005) 837–843 doi:10.1088/0953-8984/17/6/005

A new interatomic potential for the ferroelectric and paraelectric phases of $LiNbO_3$

Robert A Jackson[1] **and Mário E G Valerio**[2]

[1] Lennard-Jones Laboratories, School of Chemistry and Physics, Keele University, Keele, Staffordshire ST5 5BG, UK
[2] Physics Department, Federal University of Sergipe, Campus Universitario, 49100-000 São Cristovão, SE, Brazil

E-mail: r.a.jackson@chem.keele.ac.uk and mvalerio@fisica.ufs.br

Received 10 November 2004, in final form 10 November 2004
Published 28 January 2005
Online at stacks.iop.org/JPhysCM/17/837

Abstract

This paper reports a new interatomic potential for lithium niobate, which has been fitted to the structure and properties of the stoichiometric ferroelectric phase of the material. The potential is based on a fully ionic description of the material, with the shell model being used for the oxygen ions and a three-body potential representing the interactions of the niobium ions with the neighbouring oxygen ions. The potential set has been tested on the paraelectric phase, whose structure it reproduced to within a few per cent. The calculation of lattice properties including elastic constants and dielectric constants, as well as powder x-ray diffraction patterns of both phases, are reported.

1. Introduction

Lithium niobate, $LiNbO_3$, is a ferroelectric material with many important technological applications due to its diverse physical properties which lead to its use in elastic, elasto-optic, opto-electronic, non-linear optic and photorefractive devices [1–4]. In order to be able to understand and optimize these applications, a detailed understanding of the material properties at the atomic level is essential, and computer modelling can play an important role here. For the past 15 years or so, the principal interatomic potential available for use in atomistic simulations of the material has been the one due to Donnerberg, Tomlinson, Catlow and co-workers [5–7], hereafter referred to as the Donnerberg potential. However, since this potential was published, much new data have become available on $LiNbO_3$, as well as software for modelling temperature and pressure effects, and this has provided the motivation for the development of a new interatomic potential capable of reproducing and interpreting these data.

Table 1. Parameters of the new $LiNbO_3$ potential.

Interaction	A (eV)	ρ (Å)	C (eV Å^6)
Nb_{core}–O_{shell}	1 425.0	0.3650	0.0
Li_{core}–O_{shell}	950.0	0.2610	0.0
O_{shell}–O_{shell}	22 764.0	0.1490	27.88
Shell parameters	Shell charge, Y ($\|e\|$)	Spring constant, k_r (eV Å^{-2})	
O^{2-}	−2.9	70.0	
Three-body parameters	Force constant, k_θ (eV rad^{-2})	Equilibrium angle, θ_0 (deg)	
O_{shell}–Nb_{core}–O_{shell}	0.5776	90.0	

2. Developing the new potential

The new potential was obtained by simultaneously fitting to the structures of $LiNbO_3$ [8], Li_2O [9] and Nb_2O_5 [10], using the free energy option in the GULP code [14] at 293 K. In fitting the potential, the O^{2-}–O^{2-} potential due to Catlow [11] was retained, to make the overall potential compatible with many other oxide potentials. The reason for including Li_2O and Nb_2O_5 in the fit was to provide an additional test of the potential, and also to ensure that these materials could be used consistently in defect calculations later. The potential model employed is of the standard form adopted for inorganic materials, and has the following features: (i) Buckingham potentials between Nb–O, Li–O and O–O, (ii) fully ionic charges on Nb, Li and O with a shell model description of O, and (iii) a three-body potential describing the bonding between each Nb and its nearest O neighbours. It includes most of the same interactions as the Donnerberg potential except that in the new potential, Nb^{5+} is treated as a rigid ion, since it is hard to justify the use of the shell model on physical grounds, and there was found to be no need to include an extra quartic term in the shell model description of O^{2-}. The potential form is given below, and the parameters are listed in table 1.

(i), (ii) Buckingham potential plus electrostatic potential (Nb–O, Li–O and O–O):

$$V = q_1 q_2 / r + A \exp(-r/\rho) - C r^{-6}$$

where q_1 and q_2 are the interacting ion charges, and A, ρ and C are adjustable parameters (see table 1)

(iii) three-body potential (O–Nb–O):

$$V_{3\text{-body}} = 1/2k(\theta - \theta_0)^2$$

where θ_0 is the equilibrium bond angle and k_θ is the bond-bending force constant (see table 1).

3. Testing the potential

3.1. Ferroelectric and paraelectric structures

The potential was used to calculate the structure of both the ferroelectric [8] and paraelectric [12] phases at two temperatures, 0 K and room temperature (293 or 295 K depending on the structure determination), which was compared with the structure calculated using the Donnerberg potential. The results are given in table 2, where it is seen that the agreement obtained using the new potential is good in all cases (around 1% for the room

Table 2. Comparison of calculated and experimental structures.

	Ferroelectric phase ($R3c$)				
		New potential		Donnerberg potential	
Structural parameters	Exp. [8]	0 K	295 K	0 K	295 K
$a = b$ (Å)	5.1474	5.1559	5.1868	5.2271	5.2631
c (Å)	13.8561	13.6834	13.7103	14.2730	14.2167
z (Li)	0.2787	0.3520	0.2884	0.3618	0.3037
x (O)	0.0476	0.0525	0.0563	0.0605	0.0601
y (O)	0.3433	0.3643	0.3627	0.3498	0.3478
z (O)	0.0634	0.1328	0.0700	0.1162	0.0618
	Paraelectric phase ($R\bar{3}c$)				
		New potential		Donnerberg potential	
Structural parameters	Exp. [12]	0 K	293 K	0 K	293 K
$a = b$ (Å)	5.2924	5.1530	5.0919	2.3030	2.3042
c (Å)	13.8462	13.8418	13.2111	5.6412	5.6402
z (Li)	1/4	1/4	1/4	1/4	1/4
x (O)	0.0598	0.0342	0.0529	0.1667	0.1667
y (O)	1/3	1/3	1/3	1/3	1/3
z (O)	1/12	1/12	1/12	1/12	1/12

Table 3. Variation of lattice parameter with temperature.

T (K)	a_{exp} (Å)	a_{calc} (Å)	Δa (%)	c_{exp} (Å)	c_{calc} (Å)	Δc (%)	Exp. reference
0	—	5.155 93		—	13.683 43		
10	—	5.174 5		—	13.703 46		
295	5.147 39	5.186 78	0.77	13.856 14	13.710 25	−1.06	[8]
297	5.148 3	5.186 42	0.74	13.863 1	13.710 12	−1.10	[13]
523	5.17	5.213 25	0.84	13.87	13.719 97	−1.08	[13]

temperature structure), and it is also noted that the Donnerberg potential is unable to reproduce the paraelectric structure, while the new potential successfully reproduces the structure to around 4%, which is reasonable in view of the fact that it was not fitted to this structure. It is also interesting to consider the calculated lattice free energies of the two phases: using the new potential these are −175 and −173 eV respectively at room temperature, giving the correct relative stability of the two phases at this temperature. Considering the atomic positions, on average the new potential also gives better agreement with the experimental values (see table 2).

The new potential was also tested by calculating the lattice parameters as a function of temperature, and then comparing these with available experimental data. In table 3, the comparison is shown, and agreement between calculated and experimental structures is around 1% in all cases. It was also noted that the Donnerberg potential was not capable of reproducing the structure at 523 K. The new potential is therefore shown to be capable of modelling the structures at a range of temperatures above 0 K, important for understanding some device applications.

3.2. Elastic, dielectric and piezoelectric constants

Table 4 gives a comparison of calculated and experimental elastic, dielectric and piezoelectric constants. The calculations have been performed at two temperatures, 0 and 295 K. The Donnerberg values were recalculated using the free energy option in the GULP code [14], rather than just quoting the values directly from their papers. This was done because these values were originally calculated using a different code, which did not permit the use of free energy, and therefore did not include a full treatment of temperature effects. First, concerning the elastic constants, it is noted that the new potential generally gives a better agreement overall than the previous potential, and reproduces the trends in their relative values correctly. For example, c_{13} is now positive. In the case of c_{14}, it is noted that the experimental value is positive, but small in magnitude compared to the other elastic constants. Both potentials obtained a small negative value for this constant, which can be explained in terms of the relative weighting of this property in the fitting process.

For the static dielectric constants, $\varepsilon_{ij}(0)$, in most cases two sets of experimental values have been given in the table. These correspond to different measuring methods, in which either the crystal is unclamped, giving constant stress values, or clamped, giving constant strain values. The constant $\varepsilon_{11}(0)$ is most affected by the measurement method, while the $\varepsilon_{33}(0)$ values are less affected, as seen in the table. This had led to some confusion, because it is sometimes unclear which experimental values are being quoted in the literature. In addition, it is not possible to mimic exactly either experimental approach using the available modelling methods. For this reason, comparing experimental and calculated values is not meaningful, and the best that can be expected is that the trends be reproduced, which was achieved by both the new potential and the Donnerberg potential. It is noted that in this particular case the Donnerberg potential gives better agreement.

For the high frequency dielectric constants, $\varepsilon_{ij}(\infty)$, neither of the potentials gives good agreement with the experimental values, but the new potential gets the trend in values right, although the difference in the calculated values is small.

The piezoelectric constants d_{ij} are also given in table 4. It is noted that the calculated values are true predictions, in the sense that they were not used in fitting the new potential. The new potential reproduces d_{15} very well, and gives the correct sign for d_{22}. However, neither potential is capable of giving overall good agreement.

3.3. X-ray diffraction patterns

As a further test of the new potential, the powder x-ray diffraction pattern was calculated for the relaxed ferroelectric structure at 0 and 295 K, using the PowderCell code [22], with Cu Kα radiation in Bragg–Brentano geometry. This was compared with a pattern generated using the refined structure obtained by Abrahams and Marsh [8] (see figure 1). In figure 2, the relaxed structure obtained using the Donnerberg potential is similarly compared. It is clear from the two figures that the structures generated using the new potential are much closer to the experimental structure.

4. Conclusions

In conclusion, a new potential has been derived for $LiNbO_3$, which gives a good description of the structure and properties of both the ferroelectric and paraelectric phases, and which works over a range of temperatures. The main motivation for this work is to be able to model the full range of intrinsic and extrinsic defects that control most of the important properties of

Table 4. Comparison of experimental and calculated lattice properties. In the static dielectric constants, (u) means 'unclamped', and (c) means 'clamped' (see text for explanation).

	Present work		Donnerberg			
Parameters	0 K	295 K	0 K	295 K	Exp.	Reference
c_{11} (10^{11} N m^{-2})	2.8	2.6	0.94	0.87	2.03	[15, 16]
					2.0	[17]
					2.06	[18]
					1.9883	[1]
c_{12} (10^{11} N m^{-2})	0.63	0.49	0.60	0.37	0.573	[15]
					0.53	[16]
					0.54	[17]
					0.5464	[1]
c_{13} (10^{11} N m^{-2})	1.0	0.89	−0.23	−0.32	0.752	[15]
					0.75	[16]
					0.6	[17]
					0.6823	[1]
c_{14} (10^{11} N m^{-2})	−0.31	−0.31	−0.11	−0.39	0.089	[15]
					0.09	[16]
					0.08	[17]
					0.0783	[1]
c_{33} (10^{11} N m^{-2})	3.2	3.1	1.5	1.4	2.424	[15]
					2.45	[16]
					2.43	[17]
					2.36	[18]
					2.3571	[1]
c_{44} (10^{11} N m^{-2})	1.4	1.3	0.23	−0.67	0.595	[15]
					0.6	[16, 17]
					0.5986	[1]
$\varepsilon_{11(0)}$	12	13.4	16.2	42.8	85.2(u), 44.3(c)	[16]
					84(u), 44(c)	[19]
					84.6(u)	[15]
					43.9(c)	[20]
					84.1(u), 46.5(c)	[21]
					45.5(c)	[1]
$\varepsilon_{33}(0)$	13	13.2	15.7	18.4	28.7(u), 27.9(c)	[16]
					30(u), 29(c)	[19]
					28.6(u)	[15]
					23.7(c)	[20]
					28.1(u), 27.3(c)	[21]
					26.2(c)	[1]
$\varepsilon_{11}(\infty)$	2.42	2.40	1.87	2.04	4.905	[4]
$\varepsilon_{33}(\infty)$	2.41	2.39	1.72	2.09	4.582	[4]
d_{15} (10^{-11} C N^{-1})	5.8	7.8	148.3	−79.4	6.92	[15]
					6.8	[16]
					7.4	[20]
d_{22} (10^{-11} C N^{-1})	0.32	0.13	−28.2	40.1	2.08	[15]
					2.1	[16, 20]
d_{31} (10^{-11} C N^{-1})	2.3	3.4	12.5	22.3	−0.085	[15]
					−0.81	[16]
					−0.087	[20]
d_{33} (10^{-11} C N^{-1})	−2.7	−2.3	15.1	25.3	0.6	[15, 16]
					1.6	[20]

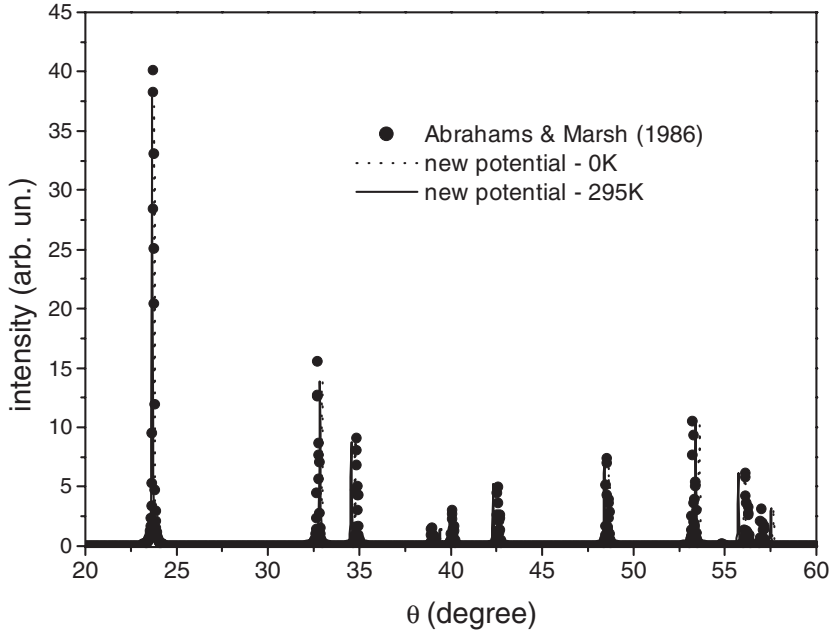

Figure 1. Calculated x-ray powder diffraction pattern generated using the new potential compared with the refined experimental structure.

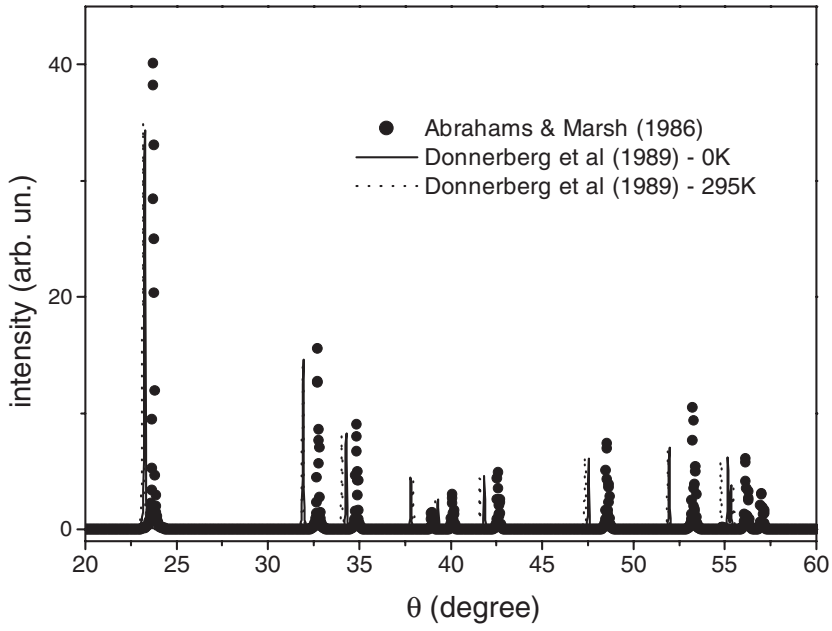

Figure 2. Calculated powder diffraction pattern generated using the Donnerberg potential compared with the refined experimental structure.

this material. Calculations of these properties are in progress and will be reported in future publications.

Acknowledgments

The authors are grateful to the CNPq, FAP-SE, CAPES and the British Council for financial support. They are also very grateful for the encouragement received from many people to carry out this work. In particular, they acknowledge many useful discussions with Drs V Dierolf, L Kovacs and G Malovichko, and Professors A V Chadwick and O F Schirmer.

References

[1] Jazbinšek M and Zgonik M 2002 *Appl. Phys.* B **74** 407
[2] Räuber A 1978 *Current Topics in Materials Science* vol 1, ed E Kaldis (Amsterdam: North-Holland) p 481
[3] Prokhorov A M and Kuz'minov Yu S 1990 *Physics and Chemistry of Crystalline Lithium Niobate* 1st edn (New York: Hilger)
[4] Wong K K (ed) 2004 *Properties of Lithium Niobate* (London: IEE)
[5] Tomlinson S M, Freeman C M, Catlow C R A, Donnerberg H and Leslie M 1989 *J. Chem. Soc. Faraday Trans.* II **85** 367
[6] Donnerberg H, Tomlinson S M, Catlow C R A and Schirmer O F 1989 *Phys. Rev.* B **40** 11909
[7] Tomlinson S M, Catlow C R A, Donnerberg H and Leslie M 1990 *Mol. Simul.* **4** 335
[8] Abrahams S C and Marsh P 1986 *Acta Crystallogr.* B **42** 61
[9] Zintl E, Harder A and Dauth B 1934 *Z. Elektrochem.* **40** 588
[10] Ercit T S 1992 *Phase Transit.* **38** 127
[11] Sanders M J, Leslie M and Catlow C R A 1984 *J. Chem. Soc. Chem. Commun.* 1271
[12] Boysen H and Altorfer F 1994 *Acta Crystallogr.* B **50** 405
[13] Abrahams S C, Hamilton W C and Reddy J M 1966 *J. Phys. Chem. Solids* **27** 1013
[14] Gale J D 1997 *J. Chem. Soc. Faraday Trans.* **93** 629
[15] Warner A W, Onoe M and Coquin G A 1967 *J. Acoust. Soc. Am.* **42** 1223
[16] Smith R T and Welch F S 1971 *J. Appl. Phys.* **42** 2219
[17] Nakagawa Y, Yamanouchi K and Shibayama K 1973 *J. Appl. Phys.* **44** 3669
[18] Graham R A 1977 *J. Appl. Phys.* **48** 2153
[19] Savage A 1966 *J. Appl. Phys.* **37** 3071
[20] Yamada T, Niizeki N and Toyoda H 1967 *Japan. J. Appl. Phys.* **6** 151
[21] Teague J R, Rice R R and Gerson R 1975 *J. Appl. Phys.* **46** 2864
[22] Kraus W and Nolze G *PowderCell for Windows* version 2.4, Federal Institute for Materials Research and Testing, Berlin, Germany